Journal of Applied Physics ARTICLE pubs.aip.org/aip/jap

Observation of temperature-dependent capture cross section for main deep-levels in β-Ga_2O_3

Cite as: J. Appl. Phys. **136**, 025701 (2024); doi: 10.1063/5.0209322
Submitted: 20 March 2024 · Accepted: 24 June 2024 ·
Published Online: 9 July 2024

A. A. Vasilev,[1,a)] A. I. Kochkova,[1] A. Y. Polyakov,[1] A. A. Romanov,[1] N. R. Matros,[1] L. A. Alexanyan,[1] I. V. Shchemerov,[1] and S. J. Pearton[2]

AFFILIATIONS

[1]Department of Semiconductor Electronics and Semiconductor Physics, National University of Science and Technology MISIS, Leninsky pr. 4, Moscow 119049, Russia
[2]Department of Materials Science and Engineering, University of Florida, Gainesville, Florida 32611, USA

Note: This paper is part of the special topic, Defects in Semiconductors 2024.
[a)]**Author to whom correspondence should be addressed:** AAVasilev@outlook.com

ABSTRACT

Direct observation of the capture cross section is challenging due to the need for extremely short filling pulses in the two-gate Deep-Level Transient Spectroscopy (DLTS). Simple estimation of the cross section can be done from DLTS and admittance spectroscopy data but it is not feasible to distinguish temperature dependence of pre-exponential and exponential parts of the emission rate equation with sufficient precision conducting a single experiment. This paper presents experimental data of deep levels in β-Ga_2O_3 that has been gathered by our group since 2017. Based on the gathered data, we propose a derivation of apparent activation energy (E_a^m) and capture cross section (σ_n^m) assuming the temperature dependent capture via the multiphonon emission model, which resulted in a strong correlation between E_a^m and σ_n^m according to the Meyer–Neldel rule, which allowed us to estimate low- and high-temperature capture coefficients C_0 and C_1 as well as capture barrier E_b. It also has been shown that without considering the temperature dependence of capture cross section, the experimental values of σ_n are overestimated by 1–3 orders of magnitude. A careful consideration of the data also allows to be more certain identifying deep levels by their "fingerprints" (E_a and σ_n) considering two additional parameters (E_{MN} and σ_{00}) and to verify the density functional theory computation of deep-level recombination properties.

I. INTRODUCTION

In recent years, Ga_2O_3 has been actively investigated by numerous research groups due to its promising potential for power electronics and solar-blind UV detectors.[1,2] To advance the application of gallium oxide devices, detailed studies have been conducted on crystal growth,[1,3,4] epitaxial film growth,[1] intentional doping, and electrically active defects.[3] Our emphasis has been focused on the deep-level defects investigation by capacitance spectroscopy, mainly Deep-Level Transient Spectroscopy (DLTS)[5] and Admittance Spectroscopy (AS).[6,7] These two techniques are widely used for characterizing electrically active defects by evaluating their concentration (N_t), thermal activation energy (E_a), and electron capture cross section (σ_n).

These parameters are obtained from electron detrapping-kinetics characterized by the emission rate $e_n(T)$ dependence on temperature T, as given by[5]

$$e_n(T) = \sigma_n \gamma T^2 \exp\left(-\frac{E_a}{kT}\right), \quad (1)$$

where $\gamma = 4\sqrt{6} \cdot k^2 \pi^{3/2} h^{-3} m^*$, m^* is an effective mass, T is the temperature, and k is the Boltzmann constant. Here, σ_n is assumed to be independent of the temperature.

The kinetics of many thermally activated processes in chemistry and physics, including the emission rate of carriers from deep levels, are usually calculated from so called Arrhenius plots, which allow us to extract the pre-exponential factor and activation energy as the temperature independent parameters for the sake of mathematical treatment simplification. This approach works well for simple estimation kinetics phenomena; however, if one is lacking knowledge of exact temperature dependence of pre-exponential factor and activation energy, it is not possible to reduce it to Arrhenius equation

term by term, and, therefore, the kinetics cannot be characterized with high precision. Furthermore, a capture cross section and activation energy cannot be determined accurately.

A. Meyer–Neldel rule in semiconductors

In terms of semiconductor physics, this problem was faced by Meyer and Neldel in 1937 when they proposed the empirical relationship given in Eq. (2) of the temperature dependence of pre-exponential factor for thermally activated conductivity.[8] This empirical law for the pre-exponential factor temperature dependence for thermally activated conductivity was presented and is now called the Meyer–Neldel rule (MNR),

$$\sigma_0 = \sigma_{00} \exp\left(-\frac{E_a}{E_{MN}}\right). \tag{2}$$

Various research groups confirmed this rule for carrier emission kinetics in A3B5 compounds,[9,10] ZnO, and other semiconductors.[11,12] The most reasonable physical explanation of the MNR in terms of emission rate is based on considering the total change in Gibbs energy with entropy part as attributed to vibrational entropy ΔS_{vib}. It has been concluded that vibrational entropy (estimated as rearrangement entropy of n interacting phonons of N total phonons in interaction volume) $\Delta S_{vib}/k_B = E_a/E_{MN} \cong n\ln(N/n)$ could not explain extremely small values of σ_{00} which are $\sim 10^{-23}$ cm^2, and that without accumulation of a significant amount of data, it is not clear whether new ideas on this issue will be proposed.[11]

From the theoretical side, Alkauskas *et al.* in 2014 developed[13] a theory on computing nonradiative capture cross section for deep-level transitions occurring via multiphonon emission, which gives insights on defect recombinational properties at different temperatures and allows us to identify defects from experimental data.

The current paper reveals new aspects of experimental deep-level parameters determination, provides results to verify such Density Functional Theory (DFT) defects computations, and demonstrates new data on capture coefficients for the main electron traps in β-Ga_2O_3.

II. SAMPLING

This analysis is based on DLTS and admittance spectroscopy data that has been gathered since 2017 for deep levels in a wide range of β-Ga_2O_3 samples. The studied samples of β-Ga_2O_3 were cut from various types of wafers purchased from Tamura/Novel Crystals, Inc., Tokyo, Japan: β-Ga_2O_3 (−201) and (010) oriented edge defined film-fed grown (EFG) wafers doped with Sn, unintentionally doped EFG (−201) wafer, (010) oriented EFG wafers doped with Fe and (001) orientated unintentionally doped halide vapor phase epitaxy (HVPE) grown layers on bulk n^+-EFG substrates doped with Sn.[14] Different sets of treatments were employed to understand the presence and origin of electrically active deep levels in β-Ga_2O_3. A detailed description of the experiments and results along with the depiction of the deep-level spectra could be found in our previous works.[15–21]

The sampling contains 1242 uncategorized data entities each corresponding to a single measurement of activation energy (E_a^m) and capture cross section (σ_n^m) from the Arrhenius plot in $\ln(e_n T^{-2})$ vs $1/T$ axes. The peak temperature (T_{peak}) is taken at the smallest window in the measurement and used only to improve quality of deep-level data clustering.

Up to now, a large number of groups have already done a significant work in the field of theoretical and experimental identification of electrically active defects in gallium oxide. Let us briefly describe the results of deep-level characterization that are taken as reference data in this analysis.

Center E1 (with E_a found in the range of 0.45–0.65 eV and σ_n found in the range of $0.3–7 \times 10^{-13}$ cm^2) has been introduced by H-plasma treatment,[19] proton irradiation,[18,21] and ampoule annealing in H_2.[15,22] It has been observed that the E1 is a donor, and according to the theoretical models, a possible configuration is the complex of H with shallow donors Si or Sn.[15]

Center E2 [$E_a = (0.74–0.82)$ eV, $\sigma_n = (0.6–23) \times 10^{-15}$ cm^2] is often detected in EFG, HVPE grown samples, and assigned to Fe acceptors.[23–32] The E2* centers [$E_a = (0.75–0.78)$ eV, $\sigma_n = (2–7) \times 10^{-14}$ cm^2] typically have been observed after radiation or implantation and demonstrate a linear increase with irradiation exposure.[21] This implies the possible origin of E2, which is a complex of intrinsic point defects of gallium and oxygen vacancies.[32]

For the E3 ($E_a = 1.05$ eV, $\sigma_n = 4.1 \times 10^{-13}$ cm^2) level detected in unintentionally doped EFG-grown β-Ga_2O_3, it has been suggested that the possible nature of the center is a deep donor related to Ti.[33] However, a defect with a similar E_a and σ_n tends to increase in concentration after irradiation with high-energy particles (neutrons and protons) and Ar plasma treatment.[21] So, the issue with these two interpretations could be the same as for E2 and E2* at early stages of β-Ga_2O_3 research.[32]

The E8 ($E_a = 0.28$ eV, $\sigma_n = 6 \times 10^{-18}$ cm^2) center is an intrinsic point defect or complex detected after irradiations and treatment with Ar and H plasma.[21]

A. Deep-level clustering

Data clustering was performed using a Gaussian Mixture model with variational inference algorithm.[34] This method assumes all data can be represented by a finite mixture of Gaussian distributions with unknown parameters which are determined from a variational lower boundary. The above procedure reduced the total data entities from 1242 to 1033, excluding dropouts, and produced 6 clusters assigned as main deep levels E2*, E4, E8, E1, E2, and E3. Results of data clustering can be seen in the pairwise plot in Fig. 1, where normalized distributions of σ_n^m, E_a^m, and T_{peak} for each trap are presented on the main diagonal plots and pairs of parameters plotted pairwise on off-diagonal plots.

Variances and mean values of σ_n^m, E_a^m, and T_{peak} for each deep-level can be determined from the data presented in Figs. 1(a), 1(e), and 1(i). The vertical alignment of clusters on Figs. 1(c) and 1(f) demonstrates no correlation of σ_n^m and E_a^m with T_{peak} (since σ_n^m and E_a^m are computed from Arrhenius plots in temperature ranges higher than T_{peak} variance) but there is strong correlation of σ_n^m with E_a^m on Fig. 1(b). This relationship will be used further for Eq. (2) fit and results analysis.

III. DERIVATIONS

Typically, the most straightforward and accurate way to determine capture cross section is through direct observation of capture

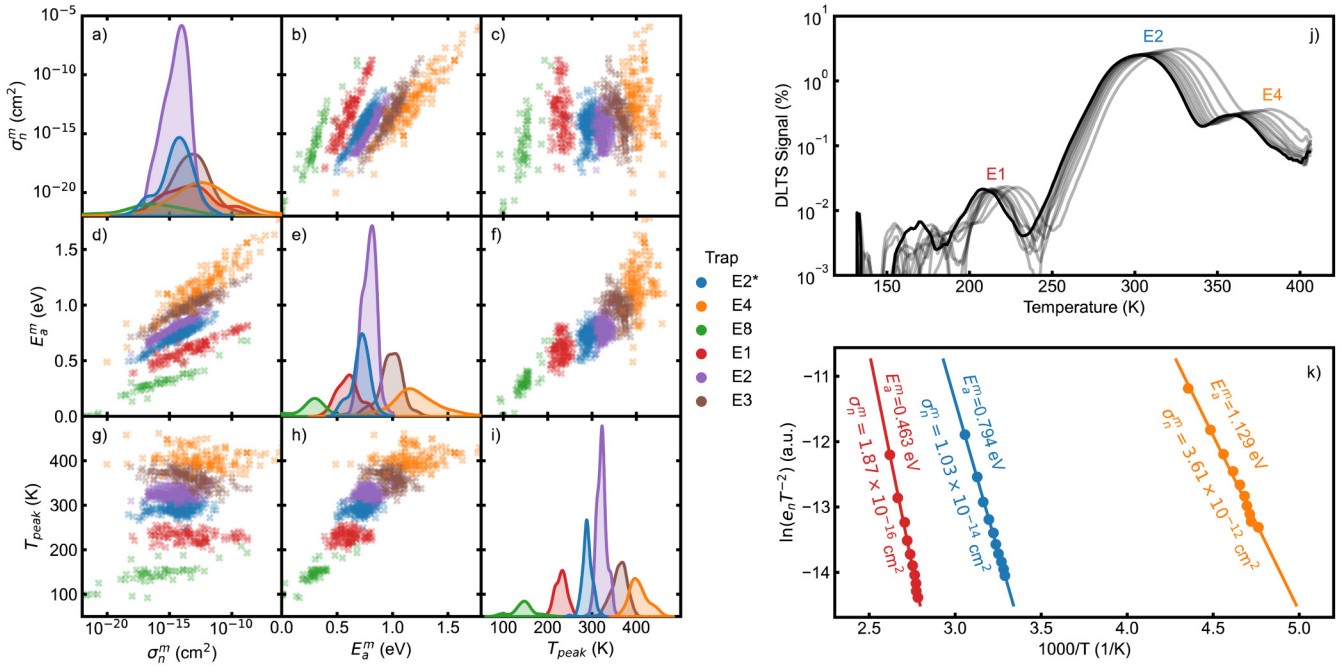

FIG. 1. Pairwise plot of clustered data for main deep levels in β-Ga_2O_3. (a), (e), and (i) Distributions of experimental parameters for trap clusters. (b), (c), (f) and (d), (g), (h) represent the same data and show the correlation within measured parameters. These scatterplots demonstrate no correlation of σ_n^m or E_a^m with T_{peak}, in which variance is determined with technique limitations. However, σ_n^m strongly depends on E_a^m and this phenomenon will be studied more thoroughly in Sec. III C below. (j) One of the DLTS measurements from the gathered data, which provides 3 of 1242 data entities represented with Arrhenius plot (k) and attributed to E1, E2, and E4 levels.

kinetics, but this method necessitates the usage of extremely short pulsing times even for materials with low doping levels in the two-gate DLTS[35] ($\tau_p^{-1} = C_n \cdot n \approx 10^{-9} \cdot 10^{15} = 1$ MHz). More simple ways are to calculate the capture cross section from standard DLTS and AS approaches,[5–7] but these techniques are not suitable for precise capture cross-section measurements, especially with the assumption of its strong temperature dependence. Emission rates can be measured by implementing long and short windows for DLTS to compute the low- and high-temperature cross section from Arrhenius plots, but in this case, it is not feasible to separate the temperature dependence of pre-exponential and exponential parts with sufficient precision conducting a single experiment.

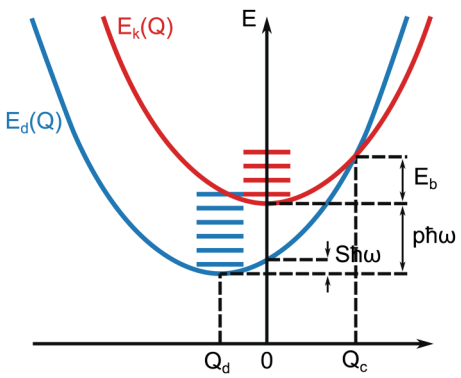

FIG. 2. Configurational diagram. E_d—energy of electron on a defect with $Q = Q_d$ (non-equal to 0 with the presence of electron–lattice interaction) and E_k—excited state that is delocalized and since then $Q = 0$ (small electron–lattice coupling to local mode Q).

Sections III A–III C will reveal a treatment of this issue, which allows to extract activation energy (E_a), low- and high-temperature capture coefficients (C_0, C_1), and capture barrier (E_b) of the deep-level through detailed DLTS and AS data analysis.

A. Vibrational entropy

The entropy term, as mentioned in the introduction, was proposed to explain the observed correlation of E_a and σ_n for other semiconductor materials. In addition, its appearance in Gibbs free energy ($-\Delta G/kT = -\Delta H/kT + \Delta S/k$) fits well with temperature independent behavior described by Eq. (2), but the vibrational entropy is relatively small $\Delta S_{vib}/k = \pm(1.5–3)$[36,37] when atomic rearrangements around defect are neglected.

B. Carrier capture by multiphonon emission

The attempt to consider coupling with local mode Q can be done with the given temperature dependence of carrier capture via multiphonon emission. The capture coefficient can be written in its low-temperature form (3),[38] with p and S defined from the configurational diagram (Fig. 2),

$$C_n \propto (\bar{n}+1)^p \frac{S^p}{p!} \exp\left(-2S\left(\bar{n}+\frac{1}{2}\right)\right). \tag{3}$$

Expression (3) can be approximated at low and high temperatures with Eq. (4),[13,38]

$$C_n(T) \approx C_0 + C_1 \exp\left(-\frac{E_b}{kT}\right). \tag{4}$$

Then, the captured cross section by definition will be

$$\sigma_n(T) = C_n(T)/\langle v_{th}\rangle, \tag{5}$$

where $\langle v_{th}\rangle = \sqrt{3kT/m^*}$ is the average thermal velocity. Thus, the temperature dependence of emission rates for carriers trapped at deep-level ($E_a = E_k(0) - E_d(Q_d)$) will be

$$e_n = \sigma_n(T) \cdot \gamma T^2 \exp\left(-\frac{E_a}{kT}\right). \tag{6}$$

Since the emission rate data from DLTS/AS experiment is treated with the Arrhenius plot, we need to analytically keep the temperature dependence of (6) until we will be ready to understand the nature of the observed E_a^m and σ_n^m correlation [Fig. 1(b)] and then simplify resulted expression in order to estimate coefficients of Eq. (4). The Arrhenius plot [Fig. 3(a)] in $\ln(e_n T^{-2})$ vs $1/T$ axes after collecting results from Eqs. (4)–(6) will be

$$\ln(e_n T^{-2}) = -\ln\langle v_{th}\rangle + \ln\gamma + \ln\left(C_0 + C_1 \exp\left(-\frac{E_b}{kT}\right)\right) - \frac{E_a}{kT}. \tag{7}$$

Therefore, apparent activation energy is computed from the slope of a tangent line at temperature T in $\ln(e_n T^{-2})$ vs $1/T$ axes. This slope as a function of temperature will be

$$\text{slope}(T) = \frac{d}{d(1/T)} \ln(e_n T^{-2}) = \frac{1}{2} T - \frac{E_b/k \cdot C_1}{C_0 e^{\frac{E_b}{kT}} + C_1} - \frac{E_a}{k}. \tag{8}$$

The corresponding intercept of a tangent line ($\text{intercept}(x) = f(x) - x \cdot f'(x)$) at temperature T, from which the apparent capture cross section is computed in $\ln(e_n T^{-2})$ vs $1/T$ axes will be

$$\text{intercept}(T) = -\ln\langle v_{th}\rangle + \ln\gamma + \ln\left(C_0 + C_1 \exp\left(-\frac{E_b}{kT}\right)\right) - \frac{E_a}{kT} - \frac{1}{T} \cdot \text{slope}(T). \tag{9}$$

Eventually, measured E_a^m and σ_n^m from slope and intercept at some temperature T will be

$$E_a^m = -\text{slope}(T) \cdot k, \tag{10}$$

$$\sigma_n^m = \frac{\exp(\text{intercept}(T))}{\gamma}. \tag{11}$$

It can be clearly seen from (8) and (10) that E_a^m appears to be step-like function [Fig. 3(b)] of T, with low- and high-temperature plateaus that are roughly E_a and $E_a + E_b$, with shift due to the presence of $-kT/2$ in E_a^m. More precise values for lower and upper boundaries are $(E_a - \Delta)$ and $(E_a + E_b - \Delta)$, where shift value Δ is $\Delta = -E_b(\ln(C_1/C_0) - 2)/(2\ln^2(C_1/C_0))$. The same temperature behavior of $\ln(\sigma_n^m)$ is presented on Fig. 3(c) with the lower and upper boundaries at the same temperatures as E_a^m.

In order to reproduce results from Fig. 1(b), the derivative of $\ln(\sigma_n^m)$ with respect to E_a^m will be

$$\frac{d(\ln(\sigma_n^m))}{dE_a^m} = \frac{(\partial \ln(\sigma_n^m)/\partial T) \cdot dT}{(\partial E_a^m/\partial T) \cdot dT} = \frac{1}{kT}. \tag{12}$$

Summing up the intermediate results, (10) and (11) imply that E_a^m and $\ln(\sigma_n^m)$ correlates through the temperature at which DLTS/AS can be performed, but experimentally we are limited in the analysis for the same reason elaborated in Sec. II A—data points from DLTS/AS data taken in broad temperature interval (around $\Delta T \approx 50$ K for E2 trap) when noticeable changes in E_a^m or $\ln(\sigma_n^m)$ are happening in a narrow temperature range. This narrow temperature range appears from data linearity in Fig. 1(b) implying by (12) [$1/kT$ should be constant or vary slowly to give linearity in Fig. 1(b)].

The gathered data for E2 trap [Figs. 3(b) and 3(c)] show that changes in $\ln(\sigma_n^m)$ occur in a narrow temperature region near some temperature T_m, so almost linear data in $\ln(\sigma_n^m)$ vs E_a^m axes will be observed. To estimate T_m, it can be assumed that $E_a^m(T_m)$ and $\sigma_n^m(T_m)$ corresponds to the middle of the step of (10) and (11) leading to the same result for T_m [Figs. 3(b) and 3(c)],

$$E_a^m(T_m) = E_a + \frac{E_b}{2} \Rightarrow T_m = \frac{E_b}{k\ln(C_1/C_0)}, \tag{13}$$

$$\frac{C_1}{C_0} \exp\left(-\frac{E_b}{kT_m}\right) = 1 \Rightarrow T_m = \frac{E_b}{k\ln(C_1/C_0)}. \tag{14}$$

Since E_a^m and $\ln(\sigma_n^m)$ data show no correlation to T_{peak} due to experiment limitations, and the biggest changes in measured parameters appear around T_m, we can expand $E_a^m(T)$ and $\ln\sigma_n^m(T)$ near T_m, excluding the temperature from equations and establishing functional dependence in form $\ln(\sigma_n^m) = f(E_a^m)$.

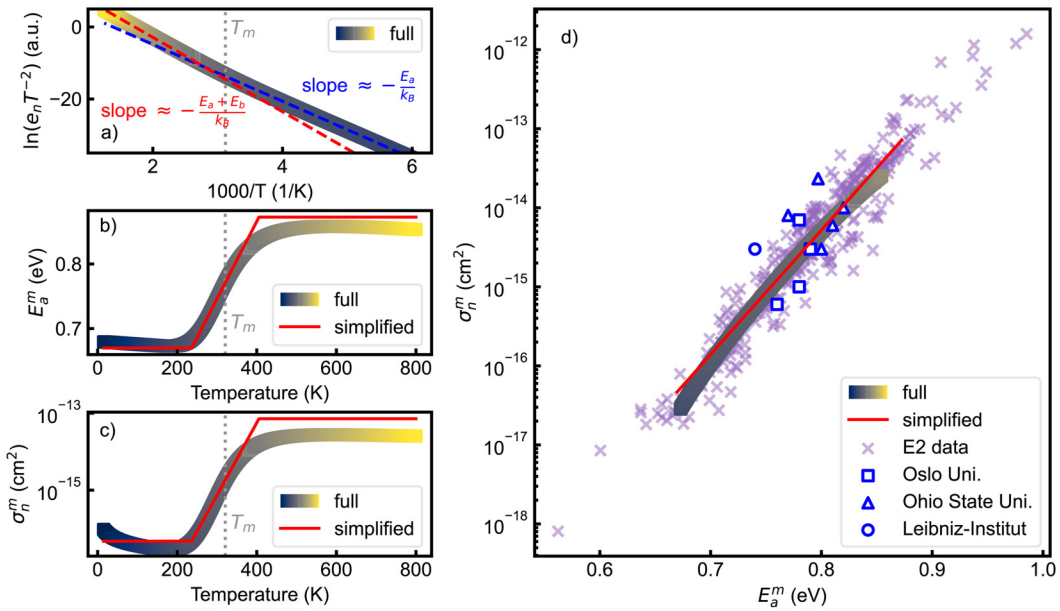

FIG. 3. Arrhenius plot and extracted parameters as a function of temperature. Fully analytical model (gradient line) with the accounting of temperature dependence of capture cross section as Eq. (5) and simplified model equation (15) (red line) of temperature dependence of measured E_a^m and σ_n^m. (a) Fully analytical Arrhenius plot showing different slope values at low and high temperatures, (b) and (c) E_a^m and σ_n^m calculated from Arrhenius plot showing step-like function, and (d) parametric plot of σ_n^m and E_a^m with full and simplified models based on our E2 data (violet crosses) and other groups' data (blue symbols).

So, expanding E_a^m at T_m up to the linear term,

$$E_a^m(T)|_{T_m} \approx E_a^m(T_m) + \frac{dE_a^m}{dT}|_{T_m}(T-T_m) + O(T^2) = E_a + E_b\left(\frac{1}{2} - \frac{\ln(C_1/C_0)}{4}\right) + kT\left(\frac{\ln^2(C_1/C_0)}{4} - \frac{1}{2}\right). \tag{15}$$

For $\ln(\sigma_n^m)$ at T_m,

$$\ln\sigma_n^m(T)|_{T_m} \approx \ln\sigma_n^m(T_m) + \frac{d\ln\sigma_n^m}{dT}|_{T_m}(T-T_m) + O(T^2) = \ln(2C_0) - \frac{1}{4}\left(\ln^2\left(\frac{C_1}{C_0}\right) - 2\ln\left(\frac{C_1}{C_0}\right)\right) - \frac{1}{2}\ln\left(\frac{3E_b}{m^*\ln(C_1/C_0)}\right) + \frac{kT}{E_b}\left(\frac{\ln^3(C_1/C_0)}{4} - \frac{\ln(C_1/C_0)}{2}\right). \tag{16}$$

Expressing and equating T from (15) and (16) brings us to $\ln(\sigma_n^m) = f(E_a^m)$ near T_m, which allows us to extract deep-level parameters from fitting the resultant expression for red line in Fig. 3,

$$f(x) = \ln(2C_0) - \frac{E_a}{E_b}\ln\left(\frac{C_1}{C_0}\right) - \frac{1}{2}\ln\left(\frac{3E_b}{m^*\ln(C_1/C_0)}\right) + x\frac{\ln(C_1/C_0)}{E_b}. \tag{17}$$

From $f(x=0)$ condition, the low-temperature capture coefficient C_0 can be estimated with experimentally known σ_{00},

$$\sigma_{00} = \frac{2C_0}{\sqrt{\frac{3kT_m}{m^*}}}\exp\left(-\frac{E_a}{kT_m}\right). \tag{18}$$

C. Model fitting

To find all four (E_a, E_b, C_0, C_1) model parameters from experimental data, it is needed to impose two more restrictions besides (13) and (18).

Assuming that enough data from many different time windows has been gathered and, therefore, the mean values of this data are represented by $E_a^m(T_m)$ and $\ln\sigma_n^m(T_m)$, the complete system of equations can be written as

$$\begin{cases} E_a + \frac{E_b}{2} \approx \text{mean}(E_a^m), & \text{(i)} \\ \log_{10}\left(\frac{2\sqrt{C_1C_0}}{\sqrt{3kT_m/m^*}}\exp(-1/2)\right) \approx \text{mean}(\log_{10}(\sigma_n^m)), & \text{(ii)} \\ \frac{E_b}{k\ln(C_1/C_0)} = T_m, & \text{(iii)} \\ \log_{10}\left(\frac{2C_0}{\sqrt{3kT_m/m^*}}\exp\left(-\frac{E_a}{kT_m}\right)\right) = \log_{10}(\sigma_{00}). & \text{(iv)} \end{cases} \tag{19}$$

This system cannot be solved analytically, so it might be suggested to use the numerical approach of finding the solution by minimizing the following function:

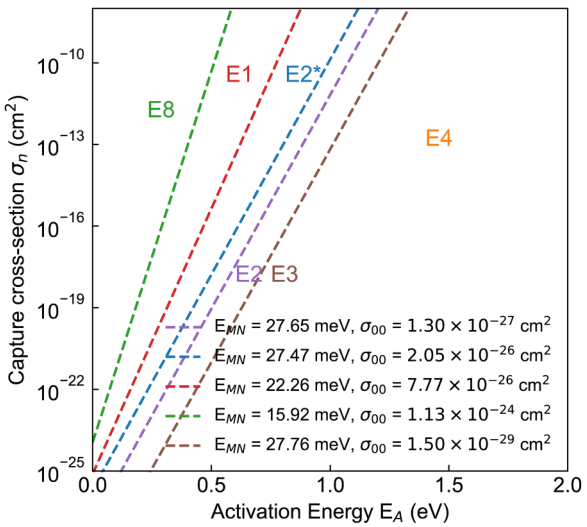

FIG. 4. Collected data on main deep levels in β-Ga_2O_3 [magnified plot from Fig. 1(b)] and fit with parameters from Table I.

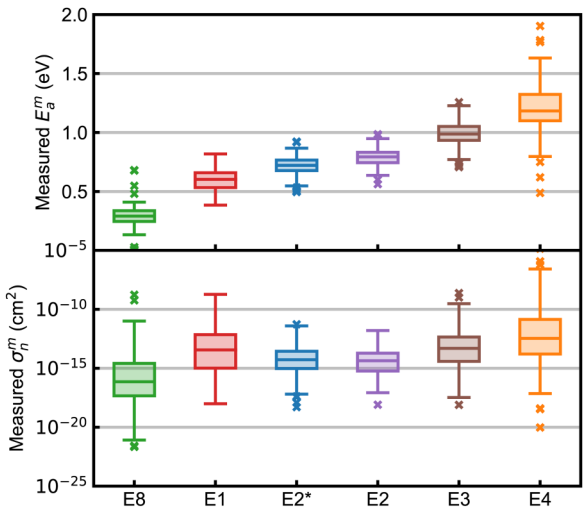

FIG. 5. E_a^m and σ_n^m distributions of main deep levels in β-Ga_2O_3, based on collected data.

$$F = \sum_{i=1}^{4} f_i - f_i^{\mathrm{RHS}}. \tag{20}$$

The corresponding solution will be

$$E_a, E_b, C_0, C_1: \quad \min_{E_a, E_b, C_0, C_1} \{\|F_2^2\|\} \leq 10^{-5}. \tag{21}$$

IV. RESULTS

Computed $E_{MN} = kT_m$ and σ_{00} for deep levels E2, E2*, E1, E8, and E3 (E4 is omitted here due to the lack of extensive collected data) in β-Ga_2O_3 are presented in Fig. 4. These data are then used for solving Eq. (21) to provide the right-hand side for Eqs. (iii) and (iv) of (19).

The distributions of gathered E_a^m and σ_n^m are represented in box-plots on Fig. 5. Boxes on Fig. 5 represent mean(E_a^m) and mean($\log_{10}(\sigma_n^m)$) at temperature T_m and used as right-hand side of Eqs. (i) and (ii) of (19). Solutions of (21) for each trap are presented in Table I and plotted in Fig. 6.

TABLE I. Results of model fitting for main deep levels in β-Ga_2O_3.

Trap	E_a (eV)	E_b (eV)	C_0 (cm^3/s)	C_1 (cm^3/s)
E2	0.68	0.21	7.0×10^{-10}	1.4×10^{-6}
E2*	0.61	0.21	1.3×10^{-9}	2.6×10^{-6}
E1	0.52	0.17	1.3×10^{-8}	3.1×10^{-5}
E8	0.23	0.12	2.0×10^{-11}	5.3×10^{-8}
E3	0.89	0.19	2.0×10^{-8}	2.0×10^{-5}

In comparison with Fig. 5, activation energies and capture cross sections obtained in experiments are overestimated due to the interplay of the temperature dependence of the capture cross section and the thermal emission terms, and, in this case, the previously measured values of the capture cross section (around T_{peak}) are 1–3 orders of magnitude higher than obtained with the suggested model.

Approaching the same problem from the theoretical side of the issue, similar results were obtained by Wickramaratne *et al.*[39] In their paper, the computed temperature dependent capture cross section via multiphonon emission mechanism was inserted into

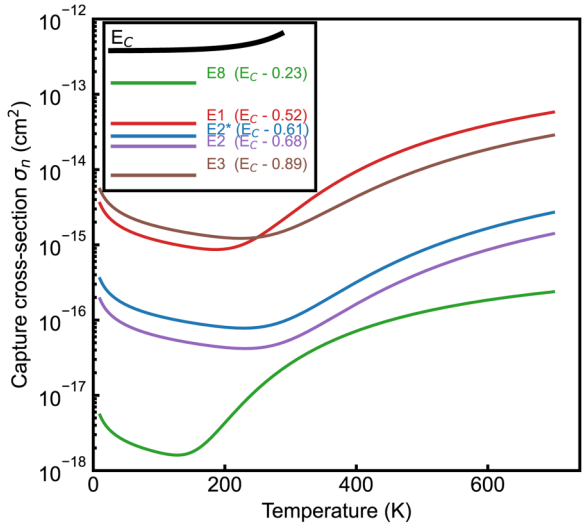

FIG. 6. Fitted model of main deep levels in β-Ga_2O_3 (data from Table I).

DLTS formalism, and it appeared to shift apparent activation energy obtained from the Arrhenius plot to higher values at higher temperatures. Nevertheless, the study[39] was not supported by any experimental data, unlike the present paper, which is possibly the first experimental observation on this matter.

V. SUMMARY AND CONCLUSIONS

In this paper, we have considered that the carrier emission rate from main deep levels in β-Ga_2O_3 follow the MN-rule and it has been shown that the capture cross section in the multiphonon emission model explains the observed E_a^m and σ_n^m shift.

We have applied the theory to the main deep-level centers in β-Ga_2O_3 and accurately calculated all parameters (Table I), including activation energy E_a, barrier height for carrier capture E_b, as well as low- and high-temperature capture coefficients C_0 and C_1.

This suggests using of E_{MN} and σ_{00} as two additional parameters to identify defects, employing C_0, C_1, and E_b to estimate capture coefficient with more detailed and advanced approach, and verifying DFT results on recombinational properties of deep levels.

ACKNOWLEDGMENTS

This research at NUST MISIS was funded by the Ministry of Science and Higher Education of the Russian Federation (Grant No. 075-15-2022-1113). This work at UF was performed as part of Interaction of Ionizing Radiation with Matter University Research Alliance (IIRM-URA), sponsored by the Department of the Defence, Defence Threat Reduction Agency under Award No. HDTRA1-20-2-0002. The content of the information does not necessarily reflect the position or the policy of the federal government, and no official endorsement should be inferred.

AUTHOR DECLARATIONS

Conflict of Interest

The authors have no conflicts to disclose.

Author Contributions

A. A. Vasilev: Conceptualization (equal); Data curation (equal); Formal analysis (equal); Investigation (equal); Methodology (equal); Software (equal); Validation (equal); Writing – original draft (equal); Writing – review & editing (equal). **A. I. Kochkova:** Conceptualization (equal); Data curation (equal); Formal analysis (equal); Investigation (equal); Methodology (equal); Validation (equal); Visualization (equal); Writing – original draft (equal); Writing – review & editing (equal). **A. Y. Polyakov:** Conceptualization (equal); Data curation (equal); Formal analysis (equal); Funding acquisition (equal); Investigation (equal); Methodology (equal); Project administration (equal); Resources (equal); Supervision (equal); Validation (equal); Visualization (equal); Writing – original draft (equal); Writing – review & editing (equal). **A. A. Romanov:** Conceptualization (equal); Data curation (equal); Formal analysis (equal); Investigation (equal); Methodology (equal); Validation (equal); Writing – original draft (equal); Writing – review & editing (equal). **N. R. Matros:** Conceptualization (equal); Data curation (equal); Formal analysis (equal); Investigation (equal); Methodology (equal); Validation (equal); Writing – original draft (equal); Writing – review & editing (equal). **L. A. Alexanyan:** Conceptualization (equal); Data curation (equal); Formal analysis (equal); Investigation (equal); Methodology (equal); Validation (equal); Writing – original draft (equal); Writing – review & editing (equal). **I. V. Shchemerov:** Conceptualization (equal); Data curation (equal); Formal analysis (equal); Investigation (equal); Methodology (equal); Validation (equal); Writing – original draft (equal); Writing – review & editing (equal). **S. J. Pearton:** Conceptualization (equal); Writing – original draft (equal); Writing – review & editing (equal).

DATA AVAILABILITY

The data that support the findings of this study are available from the corresponding author upon reasonable request.

REFERENCES

[1]M. Higashiwaki and S. Fujita, *Gallium Oxide* (Springer International Publishing, Cham, 2020).
[2]F. Ren and S. J. Pearton, *Wide Bandgap Semiconductor-Based Electronics* (IOP Publishing, 2020).
[3]E. Farzana and J. S. Speck, "Introduction," in *Ultrawide Bandgap β-Ga_2O_3 Semiconductor* (AIP Publishing LLC, 2023), pp. 1–34.
[4]N. Xia, Y. Liu, D. Wu, L. Li, K. Ma, J. Wang, H. Zhang, and D. Yang, "β-Ga_2O_3 bulk single crystals grown by a casting method," J. Alloys Compd. **935**, 168036 (2023).
[5]D. V. Lang, "Deep-level transient spectroscopy: A new method to characterize traps in semiconductors," J. Appl. Phys. **45**(7), 3023–3032 (1974).
[6]C. T. Sah, L. Forbes, L. L. Rosier, and A. F. Tasch, "Thermal and optical emission and capture rates and cross sections of electrons and holes at imperfection centers in semiconductors from photo and dark junction current and capacitance experiments," Solid State Electron. **13**(6), 759–788 (1970).
[7]G. Vincent, D. Bois, and P. Pinard, "Conductance and capacitance studies in GaP Schottky barriers," J. Appl. Phys. **46**(12), 5173–5178 (1975).
[8]W. Meyer and H. Neldel, "Relation between the energy constant and the quantity constant in the conductivity–temperature formula of oxide semiconductors," Z. Tech. Phys. **12**, 588 (1937).
[9]R. S. Crandall, "Meyer-Neldel rule in deep-level-transient-spectroscopy and its ramifications," MRS Proc. **763**, B2.5 (2003).
[10]R. S. Crandall, "Analysis of emission rate measurements in a material showing a Meyer-Neldel-rule," MRS Proc. **799**, Z1.6 (2003).
[11]Heidemarie Schmidt, Maria Wiebe, Beatrice Dittes, and Marius Grundmann, "Meyer-Neldel rule in ZnO," Appl. Phys. Lett. **91**(23), 232110 (2007).
[12]Jehad A. M. AbuShama, S. W. Johnston, R. S. Crandall, and R. Noufi, "Meyer-Neldel rule and the influence of entropy on capture cross-section determination in Cu(In,Ga)Se_2," Appl. Phys. Lett. **87**(12), 123502 (2005).
[13]A. Alkauskas, Q. Yan, and C. G. Van de Walle, "First-principles theory of nonradiative carrier capture via multiphonon emission," Phys. Rev. B **90**(7), 075202 (2014).
[14]"Tamura Corp. b-Ga_2O_3 substrates" (n.d.).
[15]A. Y. Polyakov, A. I. Kochkova, A. Langørgen, L. Vines, A. Vasilev, I. V. Shchemerov, A. A. Romanov, and S. J. Pearton, "On the possible nature of deep centers in Ga_2O_3," J. Vac. Sci. Technol. A **41**(2), 023401 (2023).
[16]A. Y. Polyakov, I.-H. Lee, N. B. Smirnov, E. B. Yakimov, I. V. Shchemerov, A. V. Chernykh, A. I. Kochkova, A. A. Vasilev, P. H. Carey, F. Ren, D. J. Smith, and S. J. Pearton, "Defects at the surface of β-Ga_2O_3 produced by Ar plasma exposure," APL Mater. **7**(6), 061102 (2019).
[17]A. Y. Polyakov, N. B. Smirnov, I. V. Schemerov, A. V. Chernykh, E. B. Yakimov, A. I. Kochkova, A. N. Tereshchenko, and S. J. Pearton, "Electrical properties, deep levels and luminescence related to Fe in bulk semi-insulating

β-Ga_2O_3 doped with Fe," ECS J. Solid State Sci. Technol. **8**(7), Q3091–Q3096 (2019).
[18]J. Kim, S. J. Pearton, C. Fares, J. Yang, F. Ren, S. Kim, and A. Y. Polyakov, "Radiation damage effects in Ga_2O_3 materials and devices," J. Mater. Chem. C **7**(1), 10–24 (2019).
[19]A. Y. Polyakov, E. B. Yakimov, V. I. Nikolaev, A. I. Pechnikov, A. V. Miakonkikh, A. Azarov, I.-H. Lee, A. A. Vasilev, A. I. Kochkova, I. V. Shchemerov, A. Kuznetsov, and S. J. Pearton, "Impact of hydrogen plasma on electrical properties and deep trap spectra in Ga_2O_3 polymorphs," Crystals **13**(9), 1400 (2023).
[20]A. Y. Polyakov, N. B. Smirnov, I. V. Shchemerov, E. B. Yakimov, J. Yang, F. Ren, G. Yang, J. Kim, A. Kuramata, and S. J. Pearton, "Point defect induced degradation of electrical properties of Ga_2O_3 by 10 MeV proton damage," Appl. Phys. Lett. **112**(3), 032107 (2018).
[21]A. Y. Polyakov, V. I. Nikolaev, E. B. Yakimov, F. Ren, S. J. Pearton, and J. Kim, "Deep level defect states in β-, α-, and ε-Ga_2O_3 crystals and films: Impact on device performance," J. Vac. Sci. Technol. A **40**(2), 020804 (2022).
[22]A. Langørgen, C. Zimmermann, Y. Kalmann Frodason, E. Førdestrøm Verhoeven, P. Michael Weiser, R. Michael Karsthof, J. Basile Varley, and L. Vines, "Influence of heat treatments in H_2 and Ar on the $E1$ center in β-Ga_2O_3," J. Appl. Phys. **131**(11), 115702 (2022).
[23]C. Zimmermann, Y. Kalmann Frodason, V. Rønning, J. B. Varley, and L. Vines, "Combining steady-state photo-capacitance spectra with first-principles calculations: The case of Fe and Ti in β-Ga_2O_3," New J. Phys. **22**(6), 063033 (2020).
[24]M. E. Ingebrigtsen, A. Y. Kuznetsov, B. G. Svensson, G. Alfieri, A. Mihaila, U. Badstübner, A. Perron, L. Vines, and J. B. Varley, "Impact of proton irradiation on conductivity and deep level defects in β-Ga_2O_3," APL Mater. **7**(2), 022510 (2019).
[25]M. E. Ingebrigtsen, L. Vines, G. Alfieri, A. Mihaila, U. Badstübner, B. G. Svensson, and A. Kuznetsov, "Bulk β-Ga_2O_3 with (010) and (201) surface orientation: Schottky contacts and point defects," Mater. Sci. Forum **897**, 755–758 (2017).
[26]E. Farzana, M. F. Chaiken, T. E. Blue, A. R. Arehart, and S. A. Ringel, "Impact of deep level defects induced by high energy neutron radiation in β-Ga_2O_3," APL Mater. **7**(2), 022502 (2019).
[27]Z. Zhang, E. Farzana, A. R. Arehart, and S. A. Ringel, "Deep level defects throughout the bandgap of (010) β-Ga_2O_3 detected by optically and thermally stimulated defect spectroscopy," Appl. Phys. Lett. **108**(5), 052105 (2016).
[28]Y.-Y. Lin, A. T. Neal, S. Mou, and J. V. Li, "Study of defects in β-Ga_2O_3 by isothermal capacitance transient spectroscopy," J. Vac. Sci. Technol. B **37**(4), 041204 (2019).
[29]H. Ghadi, J. F. McGlone, E. Cornuelle, Z. Feng, Y. Zhang, L. Meng, H. Zhao, A. R. Arehart, and S. A. Ringel, "Deep level defects in low-pressure chemical vapor deposition grown (010) β-Ga_2O_3," APL Mater. **10**(10), 101110 (2022).
[30]J. F. Mcglone, Z. Xia, Y. Zhang, C. Joishi, S. Lodha, S. Rajan, S. A. Ringel, and A. R. Arehart, "Trapping effects in Si-doped-Ga_2O_3 MESFETs on an Fe-doped-Ga_2O_3 substrate," IEEE Electron Device Lett. **39**(7), 1042–1045 (2018).
[31]K. Irmscher, Z. Galazka, M. Pietsch, R. Uecker, and R. Fornari, "Electrical properties of β-Ga_2O_3 single crystals grown by the Czochralski method," J. Appl. Phys. **110**(6), 063720 (2011).
[32]M. E. Ingebrigtsen, J. B. Varley, A. Y. Kuznetsov, B. G. Svensson, G. Alfieri, A. Mihaila, U. Badstübner, and L. Vines, "Iron and intrinsic deep level states in Ga_2O_3," Appl. Phys. Lett. **112**(4), 042104 (2018).
[33]C. Zimmermann, Y. K. Frodason, A. W. Barnard, J. B. Varley, K. Irmscher, Z. Galazka, A. Karjalainen, W. E. Meyer, F. D. Auret, and L. Vines, "Ti- and Fe-related charge transition levels in β-Ga_2O_3," Appl. Phys. Lett. **116**(7), 072101 (2020).
[34]"scikit-learn. Variational Bayesian Gaussian mixture" (n.d.).
[35]D. Pons, "Accurate determination of the free carrier capture kinetics of deep traps by space-charge methods," J. Appl. Phys. **55**(10), 3644–3657 (1984).
[36]M. Lannoo and J. Bourgoin, "Vibrational properties and entropy," (Springer, Berlin, Heidelberg, 1981), pp. 155–190.
[37]C. Lee, N. D. Rock, A. Islam, M. A. Scarpulla, and E. Ertekin, "Electron–phonon effects and temperature-dependence of the electronic structure of monoclinic β-Ga_2O_3," APL Mater. **11**(1), 011106 (2023).
[38]J. Bourgoin and M. Lannoo, "Carrier emission and recombination" (1983), pp. 154–204.
[39]D. Wickramaratne, C. E. Dreyer, B. Monserrat, J.-X. Shen, J. L. Lyons, A. Alkauskas, and C. G. Van de Walle, "Defect identification based on first-principles calculations for deep level transient spectroscopy," Appl. Phys. Lett. **113**(19), 192106 (2018).